

<https://doi.org/10.1038/s41535-024-00692-w>

# Doubled Shapiro steps in a dynamic axion insulator Josephson junction

Check for updates

Yu-Hang Li<sup>1,2,3</sup>, Zi-Qian Zhou<sup>4</sup>, Ran Cheng<sup>3,5</sup>, Hua Jiang<sup>6</sup>✉ & X. C. Xie<sup>4,6,7</sup>✉

Dynamic axion insulators feature a time-dependent axion field that can be induced by antiferromagnetic resonance. Here, we show that a Josephson junction incorporating this dynamic axion insulator between two superconductors exhibits striking doubled Shapiro steps wherein all odd steps are completely suppressed in the joint presence of a DC bias and a static magnetic field. The resistively shunted junction simulation confirms that these doubled Shapiro steps originate from the distinctive axion electrodynamics driven by the antiferromagnetic resonance, which thus not only furnishes a hallmark to identify the dynamic axion insulator but also provides a method to evaluate its mass term. Furthermore, the experimentally feasible differential conductance is also determined. Our work holds significant importance in condensed matter physics and materials science for understanding the dynamic axion insulator, paving the way for its further exploration and applications.

Axions were first introduced as a hypothetical elementary particle through the quantum field theory in high energy physics to solve the strong charge-parity problem<sup>1–3</sup>. Since electrons in the condensed system can also be described in the field operator language, the concept of axions was lately extended to condensed matter physics through the topological field theory<sup>4,5</sup>, where quasi-particle excitations in condensed system obey the axion electrodynamics, giving birth to the dynamic axion insulator that has sparked a surge of interest across multidisciplinary fields<sup>6–11</sup>. Because of the inherent dynamic axion field, DAIs possess an additional term  $\mathcal{L}_\theta = \theta(t)\alpha\mathbf{E} \cdot \mathbf{B}/\pi$  in the Lagrangian<sup>4,5</sup>, where  $\theta(t)$  is the time-dependent, massive axion field,  $\alpha$  is the fine structure constant,  $\mathbf{E}$  and  $\mathbf{B}$  are conventional magnetoelectric field. This Lagrangian introduces a magnetoelectric contribution to Maxwell's equations, making it possible to realize the axion polaritons or axion instability in condensed systems<sup>5,12,13</sup>, to drive anomalous magnetoelectric transport<sup>14,15</sup>, to detect dark matter<sup>16–19</sup>, and so on<sup>20,21</sup>.

Several candidate systems have been predicted to be DAIs<sup>14,22–27</sup>. In particular, recent first-principles calculations suggest that  $\text{Mn}_2\text{Bi}_2\text{Te}_5$  and its family, which possess coexisting antiferromagnetic ordering and topology<sup>28</sup>, may be materials of this category<sup>29,30</sup>. Since the axion field in these materials originates from the exchange interaction between topological electrons and the antiparallel magnetic moments, or the Néel vectors, the axion dynamics can then be readily achieved through the magnetic fluctuation that stimulates a time-dependent Néel vector<sup>5,29</sup>. However, because of the ultrafast dynamics of the axion field, detecting this novel state remains an outstanding challenge, thereby significantly hindering its further exploration

and potential applications. Meanwhile, there is also fierce debate about whether the magnitude of the axion mass in condensed matter materials is on the order of eV or meV<sup>31–34</sup>.

In this work, we demonstrate that this exotic quantum state can be unambiguously verified by the transport signature of a superconductor-DAI-superconductor Josephson junction. Since DAIs possess spontaneous antiferromagnetic ordering and axion field, an antiferromagnetic resonance (AFMR) can occur in DAI under the driving of a linearly polarized microwave if the microwave frequency  $\omega$  matches its intrinsic AFMR frequency<sup>35–37</sup>. In this case, the Néel vector, hence the magnetic exchange gap in the DAI, becomes time-dependent, giving rise to a dynamic axion field bound to the AFMR. The quantitative expression for this dynamic axion field turns out to be a sinusoidal function possessing a strikingly doubled frequency  $\omega_1 = 2\omega$ . Subsequently, this dynamic axion field leads to a magnetoelectric current in the presence of a static magnetic field, which becomes a harmonic supercurrent when the DAI is sandwiched between two superconductors and simultaneously, populates a coherent phase difference possessing the same doubled frequency  $\omega_1 = 2\omega$ . On the other hand, a DC bias  $V_0$  can also induce a harmonic phase difference across the Josephson junction, whose frequency is proportional to the applied bias voltage is  $\omega_2 = 2eV_0$ . Consequently, when the two frequencies  $\omega_1$  and  $\omega_2$  are commensurate with each other, such a superconductor-DAI-superconductor Josephson junction exhibits remarkable doubled Shapiro steps where all odd steps are completely suppressed. Because the magnetoelectric current originates from the axion electrodynamics driven by the AFMR, those Shapiro

<sup>1</sup>School of Physics, Nankai University, 300071 Tianjin, China. <sup>2</sup>State Key Laboratory of the Surface Physics and Department of Physics, Fudan University, 200433 Shanghai, China. <sup>3</sup>Department of Electrical and Computer Engineering, University of California, Riverside, CA, 92521, USA. <sup>4</sup>International Center for Quantum Materials, School of Physics, Peking University, 100871 Beijing, China. <sup>5</sup>Department of Physics and Astronomy, University of California, Riverside, CA, 92521, USA. <sup>6</sup>Interdisciplinary Center for Theoretical Physics and Information Sciences (ICTPIS), Fudan University, 200433 Shanghai, China. <sup>7</sup>Hefei National Laboratory, 230088 Hefei, China. ✉e-mail: [jianghuaphy@fudan.edu.cn](mailto:jianghuaphy@fudan.edu.cn); [xcxie@pku.edu.cn](mailto:xcxie@pku.edu.cn)

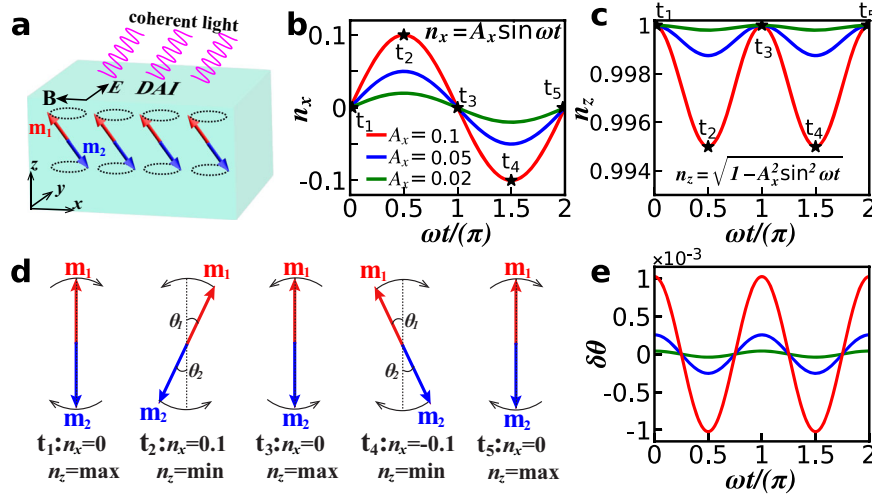


**Fig. 1 | Dynamic axion field induced by antiferromagnetic resonance in DAI.** **a** Schematic for a dynamic axion insulator driven by a linearly polarized coherent light. The arrows labeled **B** and **E** represent the magnetic and electric components of the applied light. The red and blue arrows labeled **m**<sub>1</sub> and **m**<sub>2</sub> represent the antiparallel magnetic moments forming a Néel vector, which oscillates linearly under the driving of the **B** component of the light. **b** and **c** are temporal evolutions of  $n_x$  and  $n_z$  under linearly polarized AFMR for three different amplitudes  $A_x = 0.1, 0.05, 0.02$ . The black stars mark five representative times ranging from  $t_1$  to  $t_5$ . **d** Schematics for

five representative magnetic configurations during a full circle one by one corresponding to the five times marked by black stars in **b** and **c**. The colorful arrows represent the magnetic moments **m**<sub>1</sub> (**m**<sub>2</sub>) and  $\theta_1$  ( $\theta_2$ ) denotes their polar angles. The black arrow denotes the direction of motion of the magnetic moment. The tilting angles of the Néel vector are exaggerated for clarity. **e** Temporal dependence of the dynamic axion field  $\delta\theta(t)$  obtained from Eq. (2) in the adiabatic limit at corresponding AFMR amplitudes.

steps thus not only furnish a fingerprint of DAIs but also provide a method to evaluate the axion mass.

## Results

### Effective model of the DAI

The generic low-energy effective Hamiltonian for a DAI defined on the basis of  $\psi_{\mathbf{k}} = (|p_z^+, \uparrow\rangle, |p_z^+, \downarrow\rangle, |p_z^-, \uparrow\rangle, |p_z^-, \downarrow\rangle)^T$  has the form<sup>5,29</sup>

$$\mathcal{H}(t) = \sum_{\alpha=1}^5 d_{\alpha}(\mathbf{k})\Gamma^{\alpha}, \quad (1)$$

where  $d_{1,2,3,4,5}(\mathbf{k}) = [Ak_x + m_5 n_x(t), Ak_y, Ak_z, m_0 + Bk^2, m_5 n_z(t)]$  and  $\Gamma^{1,2,3,4,5} = [\sigma_x \otimes s_x, \sigma_x \otimes s_y, \sigma_y \otimes s_x, \sigma_y \otimes s_y, \sigma_z \otimes s_z]$ . Here,  $A, B, m_0$  and  $m_5$  are system parameters.  $n_{x(z)}(t)$  denotes the  $x$ -component ( $z$ -component) of the Néel vector, which can be time-dependent in the presence of magnetic fluctuations.  $\sigma_{x,y,z}$  and  $s_{x,y,z}$  are Pauli matrices acting on the orbital and spin spaces, respectively. The lattice wave vectors  $k_{x,y,z}$  are defined in the first Brillouin zone with  $k = \sqrt{k_x^2 + k_y^2 + k_z^2}$ . The first four terms in Eq. (1) describe a topological insulator preserving both parity  $\mathcal{P} = \sigma_z$  and time reversal  $\mathcal{T} = i\tau_y \mathcal{K}$  ( $\mathcal{K}$  is the complex conjugation operator) symmetry, whose axion field is quantized to  $\theta = 0$  when  $B = 0$  while  $\theta = \pi$  otherwise<sup>5</sup>. The fifth term describes the exchange interaction between the topological electron and the dynamic, antiparallel magnetic moments, which breaks these two symmetries explicitly and thus introduces an additional dynamic part to the static axion field, giving rise to the DAI. The system parameters are generally taken as  $A = 1, B = -0.5, m_0 = 0.1, m_5 = 0.1$ . However, our theory is universal and not limited to these parameters.

### Antiferromagnetic resonance in DAIs

Under a linearly polarized microwave, an antiferromagnetic insulator resonates coherently if the frequency of the microwave is identical to its intrinsic AFMR frequency  $\omega = 2\pi\gamma\sqrt{H_A(2H_E + H_A)}$  given in Supplementary Note 1<sup>35</sup>, where  $\gamma = 28 \text{ GHz T}^{-1}$  is the gyromagnetic ratio,  $H_A$  and  $H_E$  are the uniaxial anisotropy and the exchange field between two antiparallel magnetic moments **m**<sub>1</sub> and **m**<sub>2</sub>. Although the magnetic moment, in this case, individually rotates clockwise (or counterclockwise) on an elliptical orbit, the Néel vector  $\mathbf{n} = \mathbf{m}_1 - \mathbf{m}_2$  oscillates in a purely linear mode as

schematically illustrated in Fig. 1a and c, traveling back and forth inside a perpendicular plane normal to  $\hat{y}$ -axis. Consequently,  $x$  component of the Néel vector has an explicit form  $n_x(t) = A_x \sin \omega t$  with  $A_x$  the AFMR amplitude while  $z$  component can, therefore, be analytically expressed as

$n_z(t) = \sqrt{1 - A_x^2 \sin^2 \omega t}$  since the magnitude of the Néel vector is normalized. Figure 1b and c show the temporal evolutions of  $n_x$  (b) and  $n_z$  (c), respectively, at  $A_x = 0.02, 0.05, 0.1$ . We see that the periodicity of  $n_z$  is halved compared to that of  $n_x$ , indicating that the frequency of  $n_z$  is multiplied. Since AFMR has been experimentally confirmed in  $\text{Cr}_2\text{O}_3$ <sup>36</sup> and  $\text{MnF}_2$ <sup>37</sup>, the same strategy can be conducted to trigger AFMR in antiferromagnetic  $\text{Mn}_2\text{Bi}_2\text{Te}_5$ .

### Quantitative expression for the dynamic axion field in the DAI

To establish a quantitative expression for this dynamic axion field driven by the linearly polarized AFMR, we employ the gauge-invariant expression for the axion field in terms of the Chern–Simons 3-form<sup>4</sup>. While the timescale of the AFMR, hence  $\theta(t)$ , is about seven orders of magnitude larger than the typical electron response time<sup>38</sup>, the electrons inside the DAI can adjust adiabatically to the instantaneous configuration of the Néel vector, viewing the AFMR as a static magnetic vector almost frozen in time. As a result, we can treat the DAI adiabatically<sup>39</sup>. As detailed in Supplementary Note 2, this axion field in the adiabatic limit can be calculated by using<sup>5</sup>

$$\theta = -\frac{1}{4\pi} \int d\mathbf{k}^3 \frac{2d + d_4}{(d + d_4)^2 d^3} d_5 \partial_{k_x} d_1 \partial_{k_y} d_2 \partial_{k_z} d_3, \quad (2)$$

where  $d = \sqrt{\sum_i d_i^2}$  with  $d_i$  presented in Eq. (1). Repeating this calculation at different instants of time gives the time-dependent axion field including a static part and a dynamic one, or  $\theta(t) = \theta_0 + \delta\theta(t)$ . Figure 1f plots  $\delta\theta(t)$  as a function of time at different AFMR amplitudes corresponding to Fig. 1b and c. It turns out that the temporal evolution of  $\delta\theta(t)$  is a harmonic function with a doubled frequency compared to the AFMR, that is  $\delta\theta(t) = A_{\theta} \cos 2\omega t$  where  $A_{\theta}$  is the amplitude proportional to  $A_x^2$ . These mathematical relations, especially the frequency doubling of the dynamic axion field  $\delta\theta(t)$ , are further confirmed analytically in Supplementary Note 3.

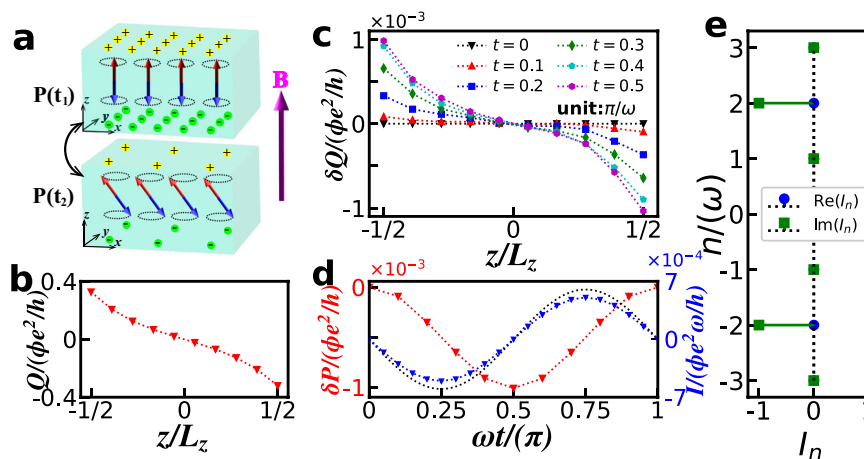


**Fig. 2 | Doubled magnetolectric current in DAI.** **a** Schematic for the instant charge polarization induced by a static magnetic field  $\mathbf{B}$  along  $\hat{z}$ -direction at  $t_1 = 0$  and  $t_2 = 2\pi/5\omega$ , respectively. The charge polarization driven by AFMR oscillates between these two values in a doubled harmonic mode. The yellow and lime spheres represent positive and negative charges, respectively. **b** Unbalanced charge distribution  $Q(z)$  at  $t_1 = 0$  for a system with size  $L_z = 10$  and  $L_y = 16$ . We use periodic boundary conditions along  $\hat{x}$ -direction. Here,  $A_x = 0.1$  and the magnetic flux inside one unit cell is  $\Phi_0 = Ba_0^2 = 0.005\phi_0$  with  $\phi_0 = h/e$  the magnetic flux quanta. **c** Increment of the charge distribution  $\delta Q(z) = Q(z, t) - Q(z, t = 0)$

ranging from  $t = 0$  to  $t = 0.5\pi/\omega$  with an interval of  $0.1\pi/\omega$  at the same parameters as the system in **(b)**. **d** Temporal evolutions of the increment of the charge polarization  $\delta P = [Q(1/2) - Q(-1/2)]/2$  obtained in the adiabatic limit from the equilibrium Green's functions provided in the “Methods” section (red inverted triangle) and the ensuing dynamic magnetolectric current calculated from the time derivative of  $\delta P$  (blue triangle). The black dashed line shows the anticipated magnetolectric current obtained from the time derivative of instant charge polarization given by Eq. (2). **e** Stem plot of the Fourier coefficients  $I_n$ .

### Dynamic magnetolectric current

Owing to the magnetolectric term in the Lagrangian  $\mathcal{L}_\theta = \theta(t)\alpha\mathbf{E} \cdot \mathbf{B}/\pi$ , the Maxwell equation acquires an additional term and thus becomes  $\nabla \cdot \mathbf{E} = \rho/\epsilon - \alpha \nabla \theta \cdot \mathbf{B}/\pi$ , where  $\epsilon$  is the permittivity and  $\rho$  is the charge density<sup>20</sup>. So a static magnetic field  $B_0$  applied to the DAI slab can induce a charge polarization given by  $P_\theta(t) = \phi\theta(t)e^2/h^{40}$ , where  $e$  is the electron charge,  $h$  is the Planck constant, and  $\phi = B_0S$  ( $S$  the area of the DAI normal to  $B_0$ ) is the magnetic flux penetrating the DAI. This charge polarization should also evolve adiabatically as the time-dependent axion field  $\theta(t)$ , leading to an equivalent magnetolectric current. At a particular instant of time, the unbalanced charge distribution illustrated in Fig. 2a can be calculated by using the lattice Green's functions provided in the “Methods” section. Figure 2b displays the unbalanced charge distribution induced by a static magnetic field along  $\hat{z}$ -direction at  $t_1 = 0$  for a system with size  $L_y = 16$ ,  $L_z = 10$  and  $A_x = 0.1$ , which corresponds to the charge polarization originating from the static axion term  $\theta_0$ . The charge distributions corresponding to  $\delta\theta(t)$  are further plotted in Fig. 2c, ranging from  $t = 0$  to  $t = \pi/2\omega$  with an interval of  $\pi/10\omega$  after subtracting the background charge distribution displayed in Fig. 2b.

Moreover, the red inverted triangle in Fig. 2d shows the instant charge polarization given by  $\delta P(t) = [\delta Q(z = -1/2) - \delta Q(z = 1/2)]/2$ , whose temporal evolution is also a harmonic function with a doubled frequency, in agreement with the dynamic axion field shown in Fig. 1e. The time derivative of this instant charge polarization gives the dynamic magnetolectric current, which is represented by the blue triangle shown in the same figure. The black dashed line is the anticipated magnetolectric current obtained from the time derivative of the dynamic axion field at  $A_x = 1$  shown in Fig. 1e and is plotted in the same figure as a benchmark. Despite the slight deviation between the two results, which can be ascribed to the finite size effect, both data can be well-fitted by using a double-frequency harmonic function. This quantitative expression of the magnetolectric current is further verified by the fast-Fourier transform shown in Fig. 2e. Since this harmonic current originates directly from the axion dynamics in DAI driven by the AFMR, it can thus stand as evidence for identifying DAIs. Nevertheless, in view of the high frequency of AFMR, which can even reach terahertz, quantitatively detecting a temporal current with such a high frequency remains a challenge.

### Doubled Shapiro steps into the DAI Josephson junction

To detect this fast dynamic magnetolectric current unique to the axion dynamics in DAI, we consider a Josephson junction consisting of a DAI sandwiched between two identical superconductors, as schematically shown in Fig. 3a. Through Andreev reflection, the dynamic magnetolectric current could stimulate a coherent phase difference across the junction, potentially synchronizing with the AC Josephson current when subjected to additional DC bias, hence becoming static transport signals termed Shapiro steps. To explore the transport properties of such a DAI Josephson junction, we employ the resistively shunted junction model illustrated in Fig. 3b, where the system is simulated as an effective circuit featuring a resistance  $R$  in parallel to the Josephson junction<sup>41</sup>. This model captures not only the tunneling electron pairs but also the leakage currents through the insulating barrier at the interfaces. The total current then comprises two components: one is the normal supercurrent  $I_0$  adjustable by applied DC bias  $V_0$  while the other is the time-dependent axion current  $I_\theta(t)$  induced by a static magnetic field  $B_0$ . Moreover, this current can be further expressed as the sum of the parallel currents in Kirchhoff's circuit, whose dynamics can be quantitatively described by the equation of motion<sup>42,43</sup>

$$I_0 + I_\theta(t) = \frac{V}{R} + I_c \sin \psi, \quad (3)$$

where  $I_0 + I_\theta(t)$  is the applied current,  $V = \hbar\dot{\psi}/2e$  is the effective voltage with  $\psi$  the phase difference across the Josephson junction and  $I_c$  is the critical supercurrent. This equation of motion can be solved numerically by using the Runge–Kutta method after substituting the dynamic current  $I_\theta(t) = -I_{ac} \sin 2\omega t$ , which is provided in the “Methods” section.

We first rewrite Eq. (3) as  $\hbar\dot{\psi}/2eR = -\partial U(\psi, t)/\partial \psi$  where  $U(\psi, t) = -[I_0 + I_\theta(t)]\psi - I_c \cos \psi$  is the washboard potential. In the absence of dynamic axion current  $I_\theta(t)$ , the static washboard potential for different  $I_0$  displayed in Fig. 3c is generally consistent with that in conventional Josephson junctions. When  $I_0 < I_c$ , the system is trapped in a local minimum, maintaining a constant phase. Increasing the current to  $I_0 = I_c$  leads to an instability responsible for the emergence of phase oscillation. The static washboard potential apparently obeys a linear

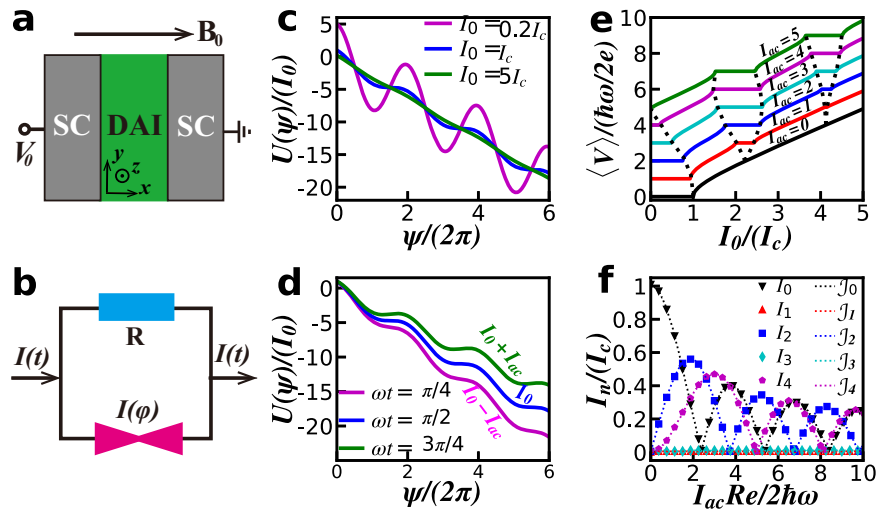


**Fig. 3 | Transport properties of a DAI Josephson junction.** **a** Schematic for a Josephson junction with a DAI sandwiched between two identical superconductors. A DC bias  $V_0$  (with the right superconductor grounded) along with a static magnetic field  $B_0$  are applied across the Josephson junction. **b** The resistively shunted junction model with an electrical resistance  $R$  shunted with the Josephson junction  $I(\psi)$ .  $I(t)$  is the total applied current. **c** and **d** are static and dynamic washboard potential versus the phase difference  $\psi$ . **e** Time-averaging voltage output as a function of the

electron current input (proportional to the DC bias  $V_0$ ) under different  $I_{ac}$  (in the unit of  $2\hbar\omega/Re$ ). Here, the data are vertically shifted one by one for clarity, and the black dashed lines that mark the boundaries of each Shapiro steps are the guide to the eye. **f** Shapiro step widths  $I_n$  as a function of  $I_{ac}$ . The markers here are obtained from the RSJ model, while the dashed lines of the same color are fitted by using the first kind of Bessel function in Eq. (4).

Ohmic relation  $I_0 = V/R$  when  $I_0 \gg I_c$ . The dynamic washboard potential for non-vanishing  $I_\theta(t)$  is presented in Fig. 3d, which oscillates between two critical boundaries represented by the green and magenta lines. This washboard potential exhibits a halved periodicity with  $T = \pi/\omega$ , in sharp contrast to conventional  $T = 2\pi/\omega$ . During one period, the system remains stable as long as the phase changes  $2n\pi$  with  $n$  an integer, resulting in a velocity  $\dot{\psi} = 2n\pi/T = 2n\omega$  in the DAI Josephson junction. As a result, the Shapiro steps emerge when the motion of the system coincides with the dynamics of the washboard potential, manifested as  $\omega_0 (= 2eV_0) = 2n\omega$ . Indeed, this washboard potential is instructive to understand the behavior of the  $I$ - $\langle V \rangle$  curve.

Figure 3e shows the  $I$ - $\langle V \rangle$  curve with different  $I_{ac}$  that is proportional to the magnetic flux  $\phi$  and thus  $B_0$ . When the magnetic field is absent,  $I_{ac} = 0$  and a typical  $I$ - $\langle V \rangle$  curve for conventional Josephson junctions without any Shapiro steps is restored as the dynamic axion current is vanishing [ $I_\theta(t) = 0$ ]. In the presence of a magnetic field ( $I_{ac} \neq 0$ ), we see that the even Shapiro steps emerge at  $\langle V \rangle = \hbar\omega/e$  while the odd steps disappear completely, in agreement with the halved periodicity in the dynamic washboard potential above. Because the voltage drop inside one Shapiro step is zero, the magnitude, also referred to as the Shapiro spike, can be obtained through the identification of the width of the plateaus at  $\langle V \rangle = \hbar\omega/2e$ , which is depicted by colorful markers in Fig. 3f as a function of  $I_{ac}$ . The result reaffirms that only doubled Shapiro steps, which evolve in perfect accordance with the Bessel functions, are sustained in the DAI Josephson junction.

**Phenomenological picture**

To understand these doubled Shapiro steps heuristically, we provide a phenomenological analysis following Barone and Paternò’s argument<sup>44</sup>. When the DAI is intimately connected to two identical superconductors, hence forming a DAI Josephson junction, the magnetoelectric current induced by applied magnetic field  $B_0$  leads to an effective bias voltage  $V_{DAI}(t) = I_\theta(t)R$  across the Josephson junction, where  $R$  is the effective resistance originating from the leakage current at the interfaces between the DAI and the superconductors. This voltage, in turn, populates a time-dependent phase difference given by Josephson’s second equation  $\Phi_\theta = \int dt V_{DAI}(t)2e/\hbar$ , which is  $\Phi_\theta = eV_1 \cos 2\omega t/\hbar$  with the effective voltage  $V_1 = I_{ac}R$ . The total phase difference across the junction,

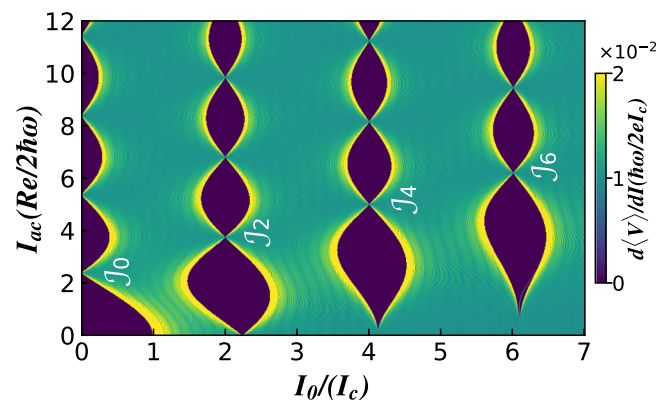


**Fig. 4 | Differential conductance of the DAI Josephson junction.** Differential conductance  $dV/dI$  on the  $I_0$ - $I_{ac}$  plane.  $I_0$  is proportional to applied DC voltage  $V_0$  while  $I_{ac}$  is proportional to applied static magnetic field  $B_0$ .  $\mathcal{J}_\alpha$  represents the first kind of Bessel function of order  $\alpha$ .

combined with an additional DC bias  $V_0$ , can thus be expressed as  $\Phi = 2eV_0t/\hbar + eV_1 \cos 2\omega t/\hbar$ . The Josephson current under such a phase difference thus reads  $I_s(t) = I_c \text{Im}\{\exp[i(2eV_0t/\hbar + eV_1 \cos 2\omega t/\hbar)]\}$  where  $I_c$  is the critical supercurrent. Applying the Jacobi–Anger expansion recasts the Josephson current as<sup>45</sup>

$$I_s(t) = I_c \sum_n \mathcal{J}_n(eV_1/\hbar\omega) \sin[(2eV_0/\hbar + 2n\omega)t], \tag{4}$$

where  $\mathcal{J}_n(x)$  is the first kind of Bessel function. Equation (4) manifestly shows that the supercurrent oscillates as a function of time unless at  $eV_0 = -n\hbar\omega$ , where doubled Shapiro steps appear with a magnitude  $I_s^n = I_c \mathcal{J}_n(eV_1/\hbar\omega)$ . To check the consistency independently, we calculate the Shapiro steps as a function of  $V_1$  by using Eq. (4) and superimpose the result as a dotted line in the same figure. We see that the two results agree with each other remarkably well, which demonstrates the consistency and reliability of the obtained results.

Finally, we determine the differential conductance  $d\langle V \rangle/dI$  on the  $I_0$ – $I_{ac}$  plane by using the resistively shunted junction simulation and show the result in Fig. 4. We observe a clear and sharp double Shapiro step pattern, where the differential conductance plateaus appear only near the location  $I_0 = 2nI_c$ . The boundaries of the plateaus marking the width of the doubled Shapiro steps coincide quantitatively with the Bessel function given in Eq. (4). This unique differential conductance pattern provides a fingerprint of the DAIs and, meanwhile, offers a platform to simulate the axion electrodynamics in condensed matter systems.

### Discussion

Despite the fact that a microwave is indispensable in both the conventional Josephson junction and the DAI Josephson junction discussed in this work, we stress that the underlying mechanisms of the doubled Shapiro steps are completely different. In conventional Josephson junctions, the microwave plays the role of a driven electric field used to induce a harmonic phase difference resonating with an additional DC bias coherently, resulting in typical Shapiro steps appearing consecutively at  $\langle V \rangle = \hbar\omega/2e$ . On the contrary, the microwave here is solely used to populate AFMR. The doubled Shapiro steps appear at  $\langle V \rangle = \hbar\omega/e$  originate from the coherence between the phase difference induced simultaneously from applied DC bias and the dynamic magnetoelectric current, which can thus be further ascribed to the axion dynamics inside DAIs. Note that our proposal is also different from the Witten effect-induced Shapiro steps predicted in ref. 46. In that work, the Josephson current originates from the charge triggered by the magnetic flux penetrating the type-II superconducting lead, which is absent in our work because the magnetic flux is fully expelled from the superconducting lead. In addition, these doubled Shapiro steps can not be ascribed to other existing mechanisms, such as the appearance of Majorana fermions<sup>47,48</sup>.

On the other hand, performing the Euler–Lagrangian equation to  $\mathcal{L}_\theta$  yields the following classical equation of motion for the dynamic axion field<sup>16,20</sup>

$$\ddot{\delta\theta} - \nabla^2\delta\theta + m_\theta^2\delta\theta = \alpha\mathbf{E} \cdot \mathbf{B}, \tag{5}$$

where  $m_\theta$  is the axion mass. Although there are ongoing debates regarding the magnitude of axion mass in condensed matter systems<sup>31–34</sup>, it is straightforward to see that the dynamic axion field induced by AFMR,  $\delta\theta(t) = A_\theta \cos 2\omega t$ , constitutes an analytical solution to Eq. (5) in a uniform system without any electromagnetic field. From this viewpoint, we obtain the axion mass  $m_\theta = 2\omega$ . Consequently, the doubled Shapiro steps proposed here also provide a method to detect the axion mass.

In  $\text{Mn}_2\text{Bi}_2\text{Te}_5$ , as the anisotropy and the exchange interaction are  $H_A = 0.8$  meV and  $H_E = 0.1$  meV<sup>49</sup>, respectively, the intrinsic AFMR frequency is  $f = \omega/2\pi \approx 143$  GHz. So the AFMR in  $\text{Mn}_2\text{Bi}_2\text{Te}_5$  can be accomplished through a linearly polarized sub-terahertz radiation of frequency 143 GHz, analogous to that in  $\text{Cr}_2\text{O}_3$ <sup>36</sup> and  $\text{MnF}_2$ <sup>37</sup>. Moreover, the typical tilting angle of the Néel vector under AFMR is about  $A_x \sim 1\%$ , in which case the amplitude of the dynamic axion field is  $A_\theta \sim 1.0 \times 10^{-5}$ . For a DAI Josephson junction with size  $S = 10^{-6}$  m<sup>2</sup> and typical contact resistance  $R \sim 10\Omega$ <sup>50</sup>, the magnitude of the required static magnetic field to observe a sizable doubled Shapiro steps is about  $B_0 \sim 0.02$  T. These can be readily achieved within current experimental technology. We thus deem that our proposal can be tested in a Josephson junction with a  $\text{Mn}_2\text{Bi}_2\text{Te}_5$  sandwiched between two conventional superconducting leads.

In summary, we have demonstrated unique doubled Shapiro steps in a superconductor–DAI–superconductor Josephson junction driven by a DC bias and a static magnetic field instead of a microwave. We ascertain that this distinctive phenomenon arises from the frequency doubling of the axion electrodynamics in DAI under the driving of a linearly polarized microwave, or alternatively from the coherent resonance between the axion mass and applied DC bias, which thus provides a fingerprint of the DAIs and can also be utilized to evaluate

the mass term of axion field in antiferromagnetic topological insulators.

### Methods

#### Lattice Hamiltonian of the DAI

The low-energy effective Hamiltonian presented in Eq. (1) can be discretized by using the  $k \cdot p$  theory. Performing the substitutions  $k_{\alpha=x,y,z} = -i\partial_\alpha \rightarrow -i(\psi_{i+\alpha} - \psi_i)/(2a_0)$  and  $k_\alpha^2 = -\partial_\alpha^2 \rightarrow -(\psi_{i+\alpha} + \psi_{i-\alpha} - 2\psi_i)/a_0^2$  with  $a_0$  the lattice constant, we can write the effective Hamiltonian as

$$\mathcal{H}(t) = \sum_{\mathbf{i}} \psi_{\mathbf{i}}^\dagger T_{\mathbf{i}}(t) \psi_{\mathbf{i}} + \left( \psi_{\mathbf{i}}^\dagger T_x \psi_{i+x} + \psi_{\mathbf{i}}^\dagger T_y \psi_{i+y} + \psi_{\mathbf{i}}^\dagger T_z \psi_{i+z} + \text{H.c.} \right), \tag{6}$$

where H.c. is the shorthand for the Hermitian conjugate, and the hopping matrices take the following form

$$\begin{aligned} T_x &= (m_0 + 6B/a_0^2)\Gamma_4 + m_5 n_x(t)\Gamma_5 + m_5 n_x(t)\Gamma_1 \\ T_x &= -iA/(2a_0)\Gamma_1 - B/a_0^2\Gamma_4 \\ T_y &= -iA/(2a_0)\Gamma_2 - B/a_0^2\Gamma_4 \\ T_z &= -iA/(2a_0)\Gamma_3 - B/a_0^2\Gamma_4, \end{aligned} \tag{7}$$

with  $n_x(t) = A_x \sin \omega t$  and  $n_z(t) = \sqrt{1 - A_x^2 \sin^2 \omega t}$ . Note that in Eq. (6), the translation symmetry along all three spatial directions in the Cartesian coordinate is well preserved.

In the presence of a static magnetic field  $\mathbf{B} = (0, 0, B)$  along  $\hat{z}$ -direction, the Hamiltonian in Eq. (6) acquires a Peierls phase  $\phi_{ij} = 2\pi \int_{\mathbf{i}}^{\mathbf{j}} \mathbf{A} \cdot d\mathbf{r}/\phi_0$  inside one unit cell from site  $\mathbf{i}$  to  $\mathbf{j}$ , where  $\mathbf{A}$  is the vector potential and  $\phi_0 = h/e$  is the magnetic flux quanta. In particular, we use the Landau gauge, therefore  $\mathbf{A} = (-yB, 0, 0)$ . The Hamiltonian thus becomes

$$\mathcal{H}(t) = \sum_{\mathbf{i}} \psi_{\mathbf{i}}^\dagger T_{\mathbf{i}}(t) \psi_{\mathbf{i}} + \left[ \psi_{\mathbf{i}}^\dagger T_x f_x(y) \psi_{i+x} + \psi_{\mathbf{i}}^\dagger T_y \psi_{i+y} + \psi_{\mathbf{i}}^\dagger T_z \psi_{i+z} + \text{H.c.} \right], \tag{8}$$

where  $f_x(y) = e^{-iyBa_0^2/\phi_0}$ .

#### Green’s functions method for calculating the charge polarization and the magnetoelectric current

Since the AFMR frequency is orders of magnitude smaller compared to the electron response time, we can treat the time-dependent AFMR adiabatically. In this case, the magnetoelectric current induced by a static magnetic field  $\mathbf{B}$  along  $\hat{z}$ -direction can be obtained from the time derivative of the instant charge polarization. Subsequently, this instant charge distribution parallel to the magnetic field can be expressed as<sup>40,51</sup>

$$q(z, t) = \frac{e}{2\pi} \sum_y \int_{-\infty}^{\epsilon_f} d\epsilon \int dk_x \text{Im}\{\text{Tr}[G^r(\epsilon, t)]\}, \tag{9}$$

where  $\epsilon_f$  is the Fermi energy and the Green’s function  $G^r(\epsilon, t) = [\epsilon + i\eta - \mathcal{H}(t)]^{-1}$  with  $\eta$  the imaginary line width function.

Moreover, Eq. (9) includes only the contribution from the negative electron charge. To obtain the unbalanced charge distribution as well as the instant charge polarization, it is necessary to include the positive background charge originating from ions that compensate for the electron charge, which has the form  $q_b = \sum_z q(z, t)/L_z$  owing to the charge conservation. As a result, the unbalanced charge distribution at time  $t$  can finally be expressed as  $Q(z, t) = q(z, t) + q_b$ .

#### Fourth-order Runge–Kutta method for solving the equation of motion of the DAI Josephson junction

For convenience, we rewritten Eq. (3) in the form  $\dot{\psi} = f(t, \psi)$  with  $f(t, \psi) = 2I_c \text{Re}(I_0/I_c - I_{ac} \sin 2\omega t/I_c - \sin \psi)/\hbar$ . This is a first-order

differential equation that can be numerically solved by using the typical Runge–Kutta method. For a step size  $h > 0$ , the phase difference  $\psi$  can be obtained iteratively by using the following equations:

$$\begin{aligned}\psi(t_{n+1}) &= \psi(t_n) + \frac{h}{8}(k_1 + 2k_2 + 2k_3 + k_4), \\ t_{n+1} &= t_n + h,\end{aligned}\quad (10)$$

where

$$\begin{aligned}k_1 &= f(t_n, \psi(t_n)), \\ k_2 &= f(t_n + h/2, \psi(t_n) + hk_1/2), \\ k_3 &= f(t_n + h/2, \psi(t_n) + hk_2/2), \\ k_4 &= f(t_n + h, \psi(t_n) + hk_3).\end{aligned}\quad (11)$$

The equation of motion can then be solved numerically by substituting the initial value  $\psi(t=0) = 0$  and  $\dot{\psi}(t=0) = 2I_0$ . The average voltage across the Josephson junction, as a function of the existing parameters  $I_0$  and  $I_{ac}$  that are adjustable through the manipulation of  $V_0$  and  $B_0$ , respectively, is then given by Josephson's second equation  $V = \int_t^{t+T} dt \dot{\psi} / 2eT$  with the period  $T = \pi/\omega$ .

### Data availability

The data that support the plots within this paper and other findings of this study are available from the corresponding authors upon request.

### Code availability

The code deemed central to the conclusions is available from the corresponding authors upon request.

Received: 12 June 2024; Accepted: 29 September 2024;

Published online: 23 October 2024

### References

- Peccei, R. D. & Quinn, H. R. CP conservation in the presence of pseudoparticles. *Phys. Rev. Lett.* **38**, 1440–1443 (1977).
- Weinberg, S. A new light boson? *Phys. Rev. Lett.* **40**, 223–226 (1978).
- Wilczek, F. Problem of strong  $p$  and  $t$  invariance in the presence of instantons. *Phys. Rev. Lett.* **40**, 279–282 (1978).
- Qi, X.-L., Hughes, T. L. & Zhang, S.-C. Topological field theory of time-reversal invariant insulators. *Phys. Rev. B* **78**, 195424 (2008).
- Li, R., Wang, J., Qi, X.-L. & Zhang, S.-C. Dynamical axion field in topological magnetic insulators. *Nat. Phys.* **6**, 284–288 (2010).
- Tokura, Y., Yasuda, K. & Tsukazaki, A. Magnetic topological insulators. *Nat. Rev. Phys.* **1**, 126–143 (2019).
- Bhattacharyya, S. et al. Recent progress in proximity coupling of magnetism to topological insulators. *Adv. Mater.* **33**, 2007795 (2021).
- Bernevig, B. A., Felser, C. & Beidenkopf, H. Progress and prospects in magnetic topological materials. *Nature* **603**, 41–51 (2022).
- Wang, P. et al. Intrinsic magnetic topological insulators. *Innovation* **2**, 100098 (2021).
- Nenno, D. M., Garcia, C. A., Gooth, J., Felser, C. & Narang, P. Axion physics in condensed-matter systems. *Nat. Rev. Phys.* **2**, 682–696 (2020).
- Rosa, P. et al. Colossal magnetoresistance in a nonsymmorphic antiferromagnetic insulator. *npj Quantum Mater.* **5**, 52 (2020).
- Ooguri, H. & Oshikawa, M. Instability in magnetic materials with a dynamical axion field. *Phys. Rev. Lett.* **108**, 161803 (2012).
- Imaeda, T., Kawaguchi, Y., Tanaka, Y. & Sato, M. Axion instability and nonlinear electromagnetic effect. *J. Phys. Soc. Jpn.* **88**, 024402 (2019).
- Sekine, A. & Nomura, K. Chiral magnetic effect and anomalous hall effect in antiferromagnetic insulators with spin–orbit coupling. *Phys. Rev. Lett.* **116**, 096401 (2016).
- Gooth, J. et al. Axionic charge–density wave in the weyl semimetal (tase4)2i. *Nature* **575**, 315–319 (2019).
- Beck, C. Possible resonance effect of axionic dark matter in Josephson junctions. *Phys. Rev. Lett.* **111**, 231801 (2013).
- Beck, C. Axion mass estimates from resonant Josephson junctions. *Phys. Dark Universe* **7–8**, 6–11 (2015).
- Klaer, V. B. & Moore, G. D. The dark-matter axion mass. *J. Cosmol. Astropart. Phys.* **2017**, 049 (2017).
- Borsanyi, S. et al. Calculation of the axion mass based on high-temperature lattice quantum chromodynamics. *Nature* **539**, 69–71 (2016).
- Sekine, A. & Nomura, K. Axion electrodynamics in topological materials. *J. Appl. Phys.* **129**, 141101 (2021).
- Xiao, Y. et al. Nonlinear level attraction of cavity axion polariton in antiferromagnetic topological insulator. *Phys. Rev. B* **104**, 115147 (2021).
- Wang, J., Li, R., Zhang, S.-C. & Qi, X.-L. Topological magnetic insulators with corundum structure. *Phys. Rev. Lett.* **106**, 126403 (2011).
- Wang, J., Lian, B. & Zhang, S.-C. Dynamical axion field in a magnetic topological insulator superlattice. *Phys. Rev. B* **93**, 045115 (2016).
- Wang, J., Lei, C., MacDonald, A. H. & Binek, C. Dynamic axion field in the magnetoelectric antiferromagnet chromia. *arXiv preprint arXiv:1901.08536* (2019).
- Zhu, T., Wang, H., Zhang, H. & Xing, D. Tunable dynamical magnetoelectric effect in antiferromagnetic topological insulator MnBi<sub>2</sub>Te<sub>4</sub> films. *npj Comput. Mater.* **7**, 121 (2021).
- Wang, H. et al. Dynamical axion state with hidden pseudospin Chern numbers in MnBi<sub>2</sub>Te<sub>4</sub>-based heterostructures. *Phys. Rev. B* **101**, 081109 (2020).
- Taguchi, K. et al. Electromagnetic effects induced by a time-dependent axion field. *Phys. Rev. B* **97**, 214409 (2018).
- Eremeev, S. V., Otrokov, M. M., Ernst, A. & Chulkov, E. V. Magnetic ordering and topology in Mn<sub>2</sub>Bi<sub>2</sub>Te<sub>5</sub> and Mn<sub>2</sub>Sb<sub>2</sub>Te<sub>5</sub> van der Waals materials. *Phys. Rev. B* **105**, 195105 (2022).
- Zhang, J. et al. Large dynamical axion field in topological antiferromagnetic insulator Mn<sub>2</sub>Bi<sub>2</sub>Te<sub>5</sub>. *Chin. Phys. Lett.* **37**, 077304 (2020).
- Cao, L. et al. Growth and characterization of the dynamical axion insulator candidate Mn<sub>2</sub>Bi<sub>2</sub>Te<sub>5</sub> with intrinsic antiferromagnetism. *Phys. Rev. B* **104**, 054421 (2021).
- Sekine, A. & Nomura, K. Axionic antiferromagnetic insulator phase in a correlated and spin–orbit coupled system. *J. Phys. Soc. Jpn.* **83**, 104709 (2014).
- Schütte-Engel, J. et al. Axion quasiparticles for axion dark matter detection. *J. Cosmol. Astropart. Phys.* **2021**, 066 (2021).
- Ishiwata, K. Axion mass in antiferromagnetic insulators. *Phys. Rev. D* **104**, 016004 (2021).
- Ishiwata, K. Topology-insensitive axion mass in magnetic topological insulators. *Phys. Rev. B* **106**, 195157 (2022).
- Kittel, C. Theory of antiferromagnetic resonance. *Phys. Rev.* **82**, 565 (1951).
- Li, J. et al. Spin current from sub-terahertz-generated antiferromagnetic magnons. *Nature* **578**, 70–74 (2020).
- Vaidya, P. et al. Subterahertz spin pumping from an insulating antiferromagnet. *Science* **368**, 160–165 (2020).
- Hassan, M. T. et al. Optical attosecond pulses and tracking the nonlinear response of bound electrons. *Nature* **530**, 66–70 (2016).
- Li, Y.-H. & Cheng, R. Spin fluctuations in quantized transport of magnetic topological insulators. *Phys. Rev. Lett.* **126**, 026601 (2021).
- Li, Y.-H. & Cheng, R. Identifying axion insulator by quantized magnetoelectric effect in antiferromagnetic MnBi<sub>2</sub>Te<sub>4</sub> tunnel junction. *Phys. Rev. Res.* **4**, L022067 (2022).
- Tinkham, M. *Introduction to Superconductivity* (Courier Corporation, 2004).

42. Heiselberg, P. *Shapiro Steps in Josephson Junctions* (Niels Bohr Institute, University of Copenhagen, 2013).
43. Stewart, W. Current-voltage characteristics of Josephson junctions. *Appl. Phys. Lett.* **12**, 277–280 (1968).
44. Antonio Barone, G. P. *Physics and Applications of the Josephson Effect* (John Wiley & Sons, Ltd, 1982).
45. Gradshteyn, I. S. & Ryzhik, I. M. *Table of integrals, series, and products* (Academic Press, 2014).
46. Nogueira, F. S., Nussinov, Z. & van den Brink, J. Josephson currents induced by the Witten effect. *Phys. Rev. Lett.* **117**, 167002 (2016).
47. Park, M. J. et al. Pressure-induced topological superconductivity in the spin-orbit mott insulator gata4se8. *npj Quantum Mater.* **5**, 41 (2020).
48. Yan, Q., Li, H., Zeng, J., Sun, Q.-F. & Xie, X. C. A Majorana perspective on understanding and identifying axion insulators. *Commun. Phys.* **4**, 239 (2021).
49. Li, Y. et al. Intrinsic topological phases in  $\text{Mn}_2\text{Bi}_2\text{Te}_5$  tuned by the layer magnetization. *Phys. Rev. B* **102**, 121107 (2020).
50. Ohkubo, M. et al. Standard measurement method for normal state resistance and critical current of resistively shunted Josephson junctions. *Supercond. Sci. Technol.* **35**, 045002 (2022).
51. Li, S., Gong, M., Li, Y.-H., Jiang, H. & Xie, X. C. High spin axion insulator. *Nat. Commun.* **15**, 4250 (2024).

## Acknowledgements

H.J. acknowledges the support from the National Key R&D Program of China (Grants Nos. 2019YFA0308403 and 2022YFA1403700) and the National Natural Science Foundation of China (Grant No. 12350401). Y.-H.L. acknowledges the support from the Fundamental Research Funds for the Central Universities and the National Natural Science Foundation of China (Grant No. 12404056). X.C.X. acknowledges the support from the Innovation Program for Quantum Science and Technology (Grant No. 2021ZD0302400). R.C. acknowledges the support from the AFOSR (Grant No. FA9550-19-1-0307). Y.-H.L. is also grateful for the financial support from the State Key Laboratory of Surface Physics and the Department of Physics at Fudan University.

## Author contributions

Y.-H.L., R.C., H.J., and X.C.X. conceived the initial idea of doubled Shapiro steps in the dynamic axion insulator Josephson junction. Y.-H.L. performed

calculations with assistance from Z.Z. Y.-H.L. wrote the manuscript with contributions from all authors. H.J. and X.C.X. supervised the project.

## Competing interests

The authors declare no competing interests.

## Additional information

**Supplementary information** The online version contains supplementary material available at <https://doi.org/10.1038/s41535-024-00692-w>.

**Correspondence** and requests for materials should be addressed to Hua Jiang or X. C. Xie.

**Reprints and permissions information** is available at <http://www.nature.com/reprints>

**Publisher's note** Springer Nature remains neutral with regard to jurisdictional claims in published maps and institutional affiliations.

**Open Access** This article is licensed under a Creative Commons Attribution-NonCommercial-NoDerivatives 4.0 International License, which permits any non-commercial use, sharing, distribution and reproduction in any medium or format, as long as you give appropriate credit to the original author(s) and the source, provide a link to the Creative Commons licence, and indicate if you modified the licensed material. You do not have permission under this licence to share adapted material derived from this article or parts of it. The images or other third party material in this article are included in the article's Creative Commons licence, unless indicated otherwise in a credit line to the material. If material is not included in the article's Creative Commons licence and your intended use is not permitted by statutory regulation or exceeds the permitted use, you will need to obtain permission directly from the copyright holder. To view a copy of this licence, visit <http://creativecommons.org/licenses/by-nc-nd/4.0/>.

© The Author(s) 2024